RESEARCH PAPER

Development and Characterization of Dual Drug–Loaded Halloysite–CMC Nanocomposites Incorporating Curcumin and Quercetin: A Novel Approach

Amol Sonawane[1*], Vaibhavi Savalia[2]

[1]Research Scholar, RK University, Bhavnagar Highway, Kasturbadham, Rajkot, Gujarat, India - 360020. Ph: +91-9743455302. Email: sonawaneamol7@gmail.com (Corresponding Author)

[2]Professor, RK University, Bhavnagar Highway, Kasturbadham, Rajkot, Gujarat, India - 360020

ABSTRACT

Curcumin (CUR) and Quercetin (QUR) are naturally occurring polyphenolic compounds widely recognized for their remarkable therapeutic potential, including antioxidant, anti-inflammatory, and anticancer activities; however, their clinical translation remains limited due to poor aqueous solubility, rapid degradation, and restricted absorption in the gastrointestinal tract, ultimately leading to very low oral bioavailability. In this research, we aimed to develop a novel formulation strategy based on halloysite nanoclay–carboxymethyl cellulose (CMC) nanocomposites co-loaded with CUR and QUR in order to enhance their solubility, stability, and dispersion characteristics. For preparation, CUR and QUR (50 mg each) were individually dissolved in ethanol and incorporated into a CMC polymeric matrix under continuous stirring to obtain CUR–CMC and QUR–CMC dispersions, which were subsequently combined with a pre-dispersed halloysite suspension to form the final nanocomposite formulations. Different halloysite-to-CMC ratios (1:1, 2:1, 3:1, and 4:1) were evaluated to optimize structural integration and drug loading efficiency. Comprehensive characterization was carried out using FTIR, XRD, DSC, and SEM techniques. FTIR analysis confirmed the presence of functional group interactions between the drug molecules and the polymer–clay matrix, indicating successful incorporation. XRD results demonstrated a marked reduction in crystallinity, suggesting improved drug dispersion within the nanocomposite system. DSC findings revealed enhanced thermal stability of the loaded compounds, while SEM micrographs showed effective embedding of the CMC matrix into the tubular halloysite structure, promoting homogeneous distribution and improved aqueous dispersibility. Overall, this formulation approach successfully addressed the intrinsic solubility limitations of CUR and QUR by providing a stable and integrated delivery platform. The halloysite–CMC nanocomposites, therefore, represent a promising system for improving the physicochemical properties, aqueous dispersion, and potential oral bioavailability of these bioactive compounds, warranting further in vivo investigations to confirm their therapeutic applicability.

Keywords: Curcumin, Quercetin, Halloysite Nanoclay, Carboxymethyl Cellulose, Nanocomposite

How to cite this article: Sonawane A, Savalia V. Development and Characterization of Dual Drug–Loaded Halloysite–CMC Nanocomposites Incorporating Curcumin and Quercetin: A Novel Approach. Int J Drug Deliv Technol. 2026;16(20s): 687-697. DOI: 10.25258/ijddt.16.20s.69

Source of support: Nil.

Conflict of interest: None

Introduction

Curcumin (CUR) and quercetin (QUR) are naturally occurring polyphenolic compounds extensively studied for their potent antioxidant, anti-inflammatory, and neuroprotective properties [1,2]. Curcumin, a bioactive compound derived from turmeric (*Curcuma longa*), has demonstrated significant therapeutic effects in various chronic diseases, including cancer, neurodegenerative disorders, and cardiovascular diseases [3,4,5]. Quercetin, a flavonoid widely present in fruits and vegetables, similarly exhibits strong free radical scavenging ability and modulates multiple signaling pathways involved in inflammation and oxidative stress [6,7]. Despite their promising bioactivities, both CUR and QUR suffer from poor water solubility and limited oral bioavailability due to low absorption, rapid metabolism, and systemic elimination [8,9]. Both curcumin and quercetin exhibit extremely low aqueous solubility, reported as less than 0.01 mg/mL for curcumin and approximately 2.15 µg/mL for quercetin at pH 7.4, which significantly limits their

dissolution and absorption [10, 11]. Although curcumin exhibits broad therapeutic potential, its clinical translation is hindered by poor aqueous solubility, rapid metabolism, and consequently low oral bioavailability, necessitating novel delivery strategies to enhance its pharmacological effectiveness [12]. The oral bioavailability of curcumin is particularly poor (<1%), with plasma concentrations often remaining in the nanomolar range even after high oral doses of 4–8 g/day [8,10]. Similarly, quercetin's reported oral bioavailability ranges from 2% to 17%, depending on its glycoside form and metabolic transformation [11,13].

These challenges significantly restrict their therapeutic potential and clinical application. Various formulation strategies such as nanoparticles, liposomes, and polymeric micelles have been explored to overcome these limitations and improve drug stability and solubility [14,15]. To overcome these bioavailability barriers, halloysite nanotubes (HNTs) have emerged as promising drug carriers due to their distinctive tubular morphology (lumen diameter 10–30 nm, outer diameter 50–70 nm, length up to 1 μm), high drug-loading efficiency (10–30%), and favorable biocompatibility profile. Nanoclay materials such as halloysite have recently gained attention as promising carriers for drug delivery due to their unique tubular morphology, biocompatibility, and ability to encapsulate both hydrophobic and hydrophilic compounds [16, 17]. Halloysite, a naturally occurring aluminosilicate clay in the form of hollow nanotubes (~50 nm outer diameter, ~15 nm lumen), has been demonstrated as an effective biocompatible nanocarrier capable of loading and controlled release of active agents [18]. Further studies have highlighted its unique nanoscale dimensions (outer diameter ~50 nm, lumen ~15 nm, length up to 900 nm) and demonstrated that its hollow lumen and end-stopper strategies enable sustained release of functional compounds over extended periods [19]. Halloysite nanotubes (HNTs) are naturally occurring, biocompatible carriers with nanoscale lumen structures that enable efficient drug encapsulation, protection against degradation, and sustained release, making them attractive, low-cost excipients for oral formulations [20]. When combined with biopolymers like carboxymethyl cellulose (CMC), halloysite-based nanocomposites can provide enhanced stability, controlled drug release, and improved dispersion of poorly soluble drugs [21]. Furthermore, combining HNTs with biopolymers like carboxymethyl cellulose (CMC) has been reported to enhance the dispersion, stability, and controlled release of poorly soluble drugs in nanocomposite systems [17,21].

This research study aims to develop and characterize dual drug-loaded nanocomposite formulations of curcumin and quercetin using halloysite nanoclay and CMC. The focus is to improve the aqueous solubility, stability, and structural integration of these phytochemicals, which may potentially overcome the challenges associated with their oral administration.

Materials and Methods

Carboxymethyl cellulose (CMC, medium viscosity), curcumin (≥95% purity), quercetin (≥98% purity), and halloysite nanoclay were procured from *Sigma-Aldrich, Mumbai, India*. Ethanol and distilled water were used as solvents and purchased from *Loba Chemie, Mumbai, India*. All chemicals and reagents were of analytical grade and used without further purification.

Physicochemical and Phytochemical Profiling

Calibration Curves for Curcumin and Quercetin

The wavelengths of maximum absorbance (λmax) for curcumin and quercetin were determined using a UV–visible spectrophotometer (Model 2600i, Shimadzu) following standard spectrophotometric protocols for polyphenolic and flavonoid compounds [30,31]. The analysis was carried out in a solvent system comprising distilled water and ethanol (1:1 v/v) and scanned over the wavelength range of 200–600 nm. The λmax values were found to be 425 nm for curcumin and 375 nm for quercetin under the selected solvent conditions. For both compounds, a primary stock solution (Stock I) was prepared by dissolving 100 mg of the respective drug in 100 mL of the solvent mixture to obtain a concentration of 1 mg/mL. From this solution, 2 mL was diluted to 100 mL with the same solvent system to prepare Stock II (20 μg/mL). Working standard solutions were then prepared by transferring 1–6 mL aliquots of Stock II into separate 10 mL volumetric flasks and diluting to volume, yielding final concentrations of 2, 4, 6, 8, 10, and 12 μg/mL. The absorbance of each solution was measured at its respective λmax against a solvent blank. Calibration curves were constructed by plotting absorbance versus concentration, and linearity was evaluated using linear regression analysis. These validated spectrophotometric methods provided the basis for quantitative estimation of

curcumin and quercetin in subsequent solubility, partition coefficient, and formulation studies [30,31].

Solubility Study

The solubility of curcumin and quercetin was determined using the equilibrium shake-flask method in distilled water and phosphate buffer solutions (pH 1.2, 6.8, and 7.4). Excess amounts of each compound were added separately to the respective media and agitated at 37 ± 0.5°C for 24 h to achieve equilibrium. The mixtures were centrifuged and filtered (0.45 µm membrane filter) to remove undissolved drug. Appropriate dilutions were prepared, and absorbance was measured using a UV–visible spectrophotometer at 425 nm for curcumin and 375 nm for quercetin. Drug concentrations were calculated using previously established calibration curves, and results were expressed as mean ± SD (n = 3).

Partition Coefficient (Log P)

Lipophilicity was evaluated by the classical shake-flask method using mutually pre-saturated n-octanol and phosphate buffer (pH 7.4) as biphasic solvents. Equal volumes of both phases were mixed with a known quantity of each compound and agitated at 25°C for 24 h to attain equilibrium. After phase separation, the drug concentration in each layer was determined spectrophotometrically at the respective λ_{max}. The partition coefficient (P) was calculated as the ratio of drug concentration in n-octanol to that in the aqueous phase, and Log P was obtained as $\log_{10} P$. Experiments were performed in triplicate.

Phytochemical Screening

Qualitative phytochemical analysis was conducted using standard tests to detect major phytoconstituents. Alkaloids (Dragendorff's, Mayer's, Hager's, Wagner's tests), carbohydrates (Molisch's, Fehling's, Benedict's tests), proteins (Biuret and Millon's tests), flavonoids (Shinoda and Ferric chloride tests), glycosides (Foam test), and phenolic compounds (Lead acetate, Ferric chloride, Bromine water, and Alkaline reagent tests) were evaluated based on characteristic color changes or precipitate formation. These studies provided essential insights into the physicochemical and phytochemical characteristics of both compounds for formulation development.

Preparation of Curcumin and Quercetin-Loaded Nanocomposites

CMC (0.25 g) was dissolved in 20 mL of distilled water by heating at 80 °C, followed by cooling to room temperature to form a clear solution. Curcumin (50 mg) was dissolved in 50 mL of ethanol and gradually added to the cooled CMC solution under continuous mechanical stirring at 1000 rpm for 1 hour, resulting in a uniform dispersion. In parallel, halloysite nanoclay (0.25 g) was dispersed in 50 mL of distilled water and stirred at 1000 rpm for 30 minutes to ensure proper dispersion. The CMC–curcumin dispersion was then slowly added to the Halloysite Suspension (HS) with continuous stirring to form the final nanocomposite formulation. To study the effect of clay-to-polymer ratio, additional formulations were prepared by maintaining the curcumin concentration constant (50 mg) while varying the HS: CMC ratios to 2:1, 3:1, and 4:1. These formulations were designated as NCCu1, NCCu2, and NCCu3, respectively.

The quercetin-loaded formulations followed the same process. CMC (0.25 g) was dissolved in 20 mL of distilled water at 80 °C and cooled to room temperature. Quercetin (50 mg) was dissolved in 50 mL of ethanol and slowly added to the CMC solution under mechanical stirring at 1000 rpm for 1 hour. Separately, 0.25 g of halloysite was dispersed in 50 mL of distilled water under the same stirring conditions. The CMC–quercetin solution was then gradually added to the clay suspension under continuous stirring to obtain the final nanocomposite. Formulations with varied HS: CMC ratios (2:1, 3:1, and 4:1) were similarly prepared and designated as NCQu1, NCQu2, and NCQu3, respectively.

Clay-to-Polymer Ratio Optimization and Drying Behavior

Nanocomposites with a 1:1 (HS: CMC) ratio exhibited poor drying behavior, with incomplete drying even after extended periods in a hot-air oven. This was attributed to the hygroscopic nature of CMC and its capacity to retain bound water, leading to prolonged moisture retention. In contrast, increasing the proportion of halloysite relative to CMC significantly improved drying efficiency. Formulations with HS: CMC ratios of 2:1, 3:1, and 4:1 dried more rapidly and uniformly, enhancing the physical handling and processability of the nanocomposites. These observations underscore the importance of optimizing the clay-to-polymer ratio in improving the practical formulation and manufacturing characteristics of nanocomposite drug delivery systems.

Formulation of Nanocomposite Tablets

Flat tablets containing nanocomposites of Curcumin (NCCu) and Quercetin (NCQu) were prepared by direct compression using 8 mm flat punches. Each tablet had a total weight of 200 mg, comprising a combination of NCCu and NCQu in equal proportions (100 mg each). Three different formulations, coded as NCQu 1, NCQu 2, and NCQu 3, were compressed following uniform processing parameters to ensure consistency in tablet dimensions and drug content.

Characterization of Nanocomposites

Optical Microscopy (Morphological Analysis)

Preliminary morphological evaluation of the drug-loaded nanocomposites was performed using an optical microscope (Model: CX23, Olympus Corporation, Japan). A small quantity of the dried sample was placed on a clean glass slide, uniformly spread, and observed under suitable magnifications (10× and 40× objectives). Particle shape, surface appearance, aggregation behavior, and homogeneity were examined and compared with those of the pure drug and physical mixtures to assess morphological changes after formulation.

Fourier Transform Infrared Spectroscopy (FTIR)

FTIR analysis was carried out using an FTIR spectrophotometer (Model: IR Affinity-1S, Shimadzu Corporation, Japan) to evaluate potential molecular interactions between the drug(s), carboxymethyl cellulose (CMC), and halloysite nanoclay. Samples of pure drug, excipients, and nanocomposites were finely mixed with potassium bromide (KBr) and compressed into pellets using a hydraulic press. Spectra were recorded over the range of 4000–400 cm^{-1} at a resolution of 4 cm^{-1}. Characteristic peaks were analyzed for shifts, disappearance, or broadening to confirm intermolecular interactions and successful incorporation into the nanocomposite matrix.

X-ray Diffraction (XRD)

XRD analysis was performed using an X-ray diffractometer (Model: XRD-7000, Shimadzu Corporation, Japan) to determine the crystalline or amorphous nature of the samples. Powdered samples were placed on the sample holder and scanned over a 2θ range of 10°–80° at a scanning rate of 2°/min using Cu-Kα radiation (λ = 1.5406 Å), operated at 40 kV and 30 mA. Diffraction patterns were evaluated for changes in peak intensity, disappearance of crystalline peaks, or halo formation, indicating modification in crystallinity and possible intercalation within the clay–polymer network.

Differential Scanning Calorimetry (DSC)

Thermal behavior of pure drug(s), excipients, and nanocomposites was analyzed using a Differential Scanning Calorimeter (Model: DSC-60 Plus, Shimadzu Corporation, Japan). Accurately weighed samples (2–5 mg) were sealed in aluminum pans and heated over a temperature range of 30–300°C at a heating rate of 10°C/min under a nitrogen purge (flow rate: 50 mL/min). Thermograms were recorded to identify melting points and thermal transitions. Changes in characteristic endothermic peaks were interpreted as evidence of drug–excipient interactions or alteration in physical state.

Scanning Electron Microscopy (SEM)

Surface morphology of the nanocomposites was examined using a Scanning Electron Microscope (Model: JSM-IT200, JEOL Ltd., Japan). Samples were mounted on aluminum stubs with double-sided carbon tape and sputter-coated with a thin layer of gold using a sputter coater (Model: JFC-1600, JEOL, Japan) to enhance conductivity. Micrographs were captured at appropriate accelerating voltages (10–20 kV) and magnifications to evaluate particle size, surface texture, homogeneity, and drug distribution within the composite system. Comparisons were made with pure drug samples to confirm structural modifications following nanocomposite formation.

In Vitro Drug Release Study of Nanocomposite Formulation

The in vitro drug release of the nanocomposite tablets was evaluated using a static dissolution method in 100 mL of ethanol and phosphate-buffered saline (PBS, pH 5.8) in a 1:1 (v/v) ratio at room temperature. Each tablet was placed in the release medium, and at predetermined time intervals, 1 mL aliquots were withdrawn and replaced with an equal volume of fresh, drug-free medium to maintain constant volume and sink conditions. The collected samples were suitably diluted and analyzed using a UV–Visible spectrophotometer by the simultaneous equation (Vierordt's) method. Absorbance was measured at 428 nm for curcumin and 372 nm for quercetin, consistent with their previously established λmax values. The recorded absorbance values were substituted into the respective simultaneous equations derived from their absorptivity coefficients to determine individual drug concentrations. The cumulative percentage drug release was calculated and plotted against time. All experiments were performed in

triplicate, and results were expressed as mean ± standard deviation.

Results and Discussion

Physicochemical and Phytochemical Profiling

Calibration Curves for Curcumin and Quercetin

The calibration curves of curcumin and quercetin were constructed in the concentration range of 2–12 µg/mL using UV–visible spectrophotometric analysis. For curcumin, absorbance was measured at λmax = 428 nm. The absorbance values increased proportionally with concentration, demonstrating a linear relationship within the studied range (Table 1, Figure 1). The mean absorbance ranged from 0.212 ± 0.012 at 2 µg/mL to 0.983 ± 0.011 at 12 µg/mL. The calibration plot of absorbance versus concentration showed good linearity with a high correlation coefficient ($R^2 \approx 0.99$), indicating compliance with Beer–Lambert's law. Similarly, for quercetin, absorbance was recorded at λmax = 372 nm. A concentration-dependent increase in absorbance was observed (Table 2, Figure 2), with mean values ranging from 0.212 ± 0.007 at 2 µg/mL to 0.982 ± 0.008 at 12 µg/mL. The regression analysis confirmed excellent linearity over the selected concentration range ($R^2 \approx 0.99$). The low standard deviation values across all concentrations indicate good precision and reproducibility of the method. These results validate the developed UV spectrophotometric methods for accurate quantitative estimation of curcumin and quercetin in subsequent solubility, partition coefficient, and formulation studies.

Table 1: UV absorbance data of curcumin at different concentrations

Absorbance (nm) at λmax = 428 nm				
Concentration	**Set 1**	**Set 2**	**Set3**	**Mean (SD)**
0	0	0	0	0
2	0.198	0.218	0.221	0.212333 (0.0125)
4	0.373	0.358	0.368	0.366333 (0.00763)
6	0.528	0.502	0.517	0.515667 (0.01305)
8	0.677	0.69	0.683	0.683333 (0.0065)
10	0.828	0.842	0.854	0.841333 (0.0130)
12	0.972	0.982	0.994	0.982667 (0.01101)

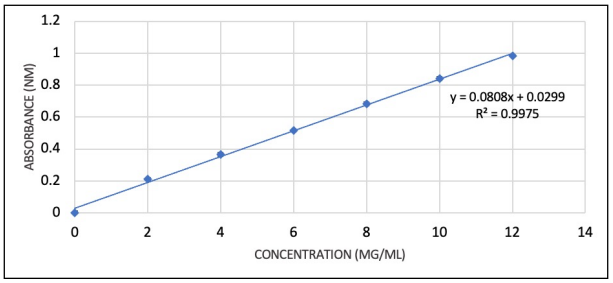

Figure 1: Calibration curve of Curcumin

Table 2: UV absorbance data of Quercetin at different concentrations

Absorbance (nm) at λmax = 372 nm				
Concentration	**Set 1**	**Set 2**	**Set3**	**Mean (SD)**
0	0	0	0	0
2	0.204	0.214	0.218	0.212 (0.007)
4	0.384	0.361	0.376	0.373 (0.011)
6	0.497	0.513	0.507	0.505 (0.008)
8	0.639	0.634	0.648	0.640 (0.007)
10	0.811	0.836	0.824	0.823 (0.012)
12	0.992	0.982	0.9743	0.982 (0.008)

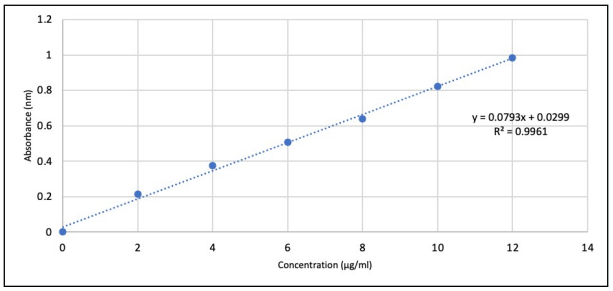

Figure 2: Calibration curve of Quercetin

Solubility Study

The saturation solubility of curcumin and quercetin was determined in ethanol and distilled water using the equilibrium shake-flask method, and the drug concentrations were quantified by UV–visible

spectrophotometry at their respective λmax values (Table 3). For curcumin (λmax = 428 nm), significantly higher solubility was observed in ethanol compared to water. The mean absorbance in ethanol was 0.248 ± 0.007, corresponding to a concentration of 3.104 mg/mL, whereas in water, the mean absorbance was 0.040 ± 0.005, corresponding to only 0.005 mg/mL. These findings confirm the poor aqueous solubility and strong lipophilic nature of curcumin. Similarly, for quercetin (λmax = 372 nm), greater solubility was observed in ethanol (mean absorbance 0.0145 ± 0.003; 1.83 mg/mL) compared to water (mean absorbance 0.0295 ± 0.004; 0.003 mg/mL). The markedly lower solubility in water further supports its limited aqueous dissolution characteristics. The low standard deviation values indicate good reproducibility of the method. Overall, both compounds exhibited substantially higher solubility in ethanol than in water, highlighting their hydrophobic nature and justifying the need for advanced formulation strategies to enhance aqueous solubility and bioavailability.

Table 3: Solubility Profile of curcumin and quercetin

Solvent	Set 1	Set 2	Set3	Mean (SD)	Conc (mg/mL)
Curcumin: Absorbance (nm) at λmax = 428 nm					
Ethanol	0.248	0.241	0.256	0.248 (0.007)	3.104
Water	0.044	0.0347	0.042	0.040 (0.005)	0.005
Quarcetin: Absorbance (nm) at λmax = 372 nm					
Ethanol	0.011	0.016	0.0166	0.0145 (0.003)	1.83
Water	0.028	0.0347	0.026	0.0295 (0.004)	0.003

Partition Coefficient

The partition coefficient (Log P) of curcumin and quercetin was determined using the classical shake-flask method with mutually saturated n-octanol and water phases. Drug concentrations in the aqueous phase were quantified by UV–visible spectrophotometry at their respective λmax values, and Log P was calculated from the ratio of concentrations in octanol and water (Table 4). For curcumin (λmax = 428 nm), the mean aqueous absorbance was 0.022 ± 0.002, corresponding to a concentration of 0.013 mg/mL, while the concentration in the octanol phase was 99.98 mg/mL. The calculated Log P value was 3.86, indicating high lipophilicity and strong preferential partitioning into the organic phase. For quercetin (λmax = 372 nm), the mean aqueous absorbance was 0.783 ± 0.002, corresponding to 0.493 mg/mL, whereas the octanol phase concentration was 99.507 mg/mL. The calculated Log P value was 2.30, suggesting moderate lipophilicity compared to curcumin. The low standard deviation values reflect good precision and reproducibility of the analytical method. Overall, the results confirm the lipophilic nature of both compounds, with curcumin exhibiting higher hydrophobicity than quercetin, which may significantly influence their membrane permeability and formulation behavior.

Table 4: Log P value for curcumin and quercetin

Solvent	Set 1	Set 2	Set 3	Mean (SD)	Conc (mg/mL)	Log p
Curcumin: Absorbance (nm) at λmax = 428 nm						
Water	0.023	0.02	0.024	0.022 (0.002)	0.013	3.86
Octanol	-	-	-	-	99.98	
Quercetin: Absorbance (nm) at λmax = 372 nm						
Water	0.779	0.787	0.783	0.783 (0.002)	0.493	2.30
Octanol	-	-	-	-	99.507	

Phytochemical Screening

Preliminary qualitative phytochemical screening of curcumin and quercetin was performed using standard chemical tests (Table 5). Both compounds showed positive results for alkaloids, as confirmed by Dragendorff's, Mayer's, Hager's, and Wagner's tests. In the flavonoid analysis, both curcumin and quercetin exhibited positive responses in the Shinoda and Ferric chloride ($FeCl_3$) tests, confirming the presence of

flavonoid moieties. For carbohydrates, both compounds gave positive results in Fehling's and Benedict's tests, while Molisch's test was negative; however, the overall observations indicated the presence of carbohydrate-related constituents. The protein tests (Biuret and Millon's) were negative for both compounds, indicating the absence of proteins. Similarly, the glycoside test (Foam test) showed negative results, confirming their absence. Strong positive responses were observed in all tests for phenolic compounds (Lead acetate, Bromine water, Ferric chloride, and Alkaline reagent tests), supporting the well-established phenolic nature and antioxidant potential of both phytoconstituents. Overall, the phytochemical screening confirms the presence of alkaloids, flavonoids, phenolics, and carbohydrates, while proteins and glycosides were absent. These findings align with the known chemical profiles of curcumin and quercetin and support their suitability for further development in nanocarrier-based drug delivery systems.

Table 5: Different Phytochemical tests

Test for Alkaloids					
Name	**Dragendorff's**	**Mayer's**	**Hager's test**	**Wagner's test:**	**Remark**
Curcumin	+ve	+ve	+ve	+ve	Present
Quercetin	+ve	+ve	+ve	+ve	Present
Test for Flavonoids					
	Shinoda Test	**FeCl test**	**Remark**		
Curcumin	+ve	+ve	Present		
Quercetin	+ve	+ve	Present		
Test for Carbohydrates					
	Molisch Test	**Fehling Test**	**Benedict's Test**	**Remark**	
Curcumin	-ve	+ve	+ve	Present	
Quercetin	-ve	+ve	+ve	Present	
Test for Protein					
	Biuret Test	**Millon's Test**	**Remark**		
Curcumin	-ve	-ve	Not- Present		
Quercetin	-ve	-ve	Not- Present		
Test for Phenolic Compound					
	Lead acetate Test	**Bromine water**	**FeCl test**	**Alkaline reagent test**	**Remark**
Curcumin	+ve	+ve	+ve	+ve	Present
Quercetin	+ve	+ve	+ve	+ve	Present
Test for Glycosides					
	Foam test Drug		**Remark**		
Curcumin	-ve		Not- Present		
Quercetin	-ve		Not- Present		

Characterization of Nanocomposites

Morphological Observation through Optical Microscopy

Optical microscopy images revealed that halloysite (HS) particles were distinctly coated with the drug-impregnated carboxymethyl cellulose (CMC) polymer. The interaction led to a visible encapsulation of clay by the polymer, forming a uniform composite structure. In formulations with higher HS content, the clay phase appeared more dominant, suggesting that the clay acted as a continuous phase in the matrix. However, even in such cases, the polymer chains effectively formed an interconnected network, embedding the clay particles densely within the structure. [fig-3-4]

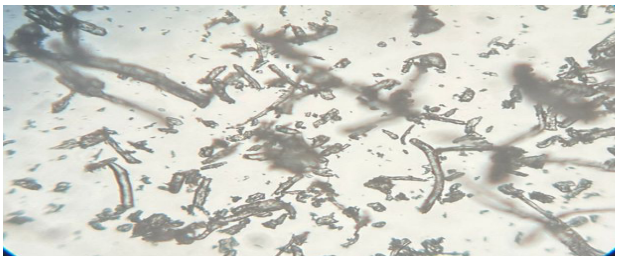

Figure 3: Morphology of curcumin

Figure 4: Morphology of quercetin

Fourier Transform Infrared Spectroscopy (FTIR)

The pure curcumin spectrum exhibits characteristic peaks corresponding to –OH stretching around 3400 cm^{-1}, C=O stretching near 1625 cm^{-1}, and aromatic C=C vibrations at approximately 1600 and 1500 cm^{-1}. In the nanocomposite formulations, these peaks show slight shifts and changes in intensity, suggesting interactions between curcumin, carboxymethyl cellulose (CMC), and halloysite clay. Notably, new peaks appearing in the 1030–1100 cm^{-1} region confirm the presence of halloysite's Si–O functional groups. These spectral modifications indicate successful incorporation of curcumin into the polymer–clay nanocomposite matrix, likely mediated by hydrogen bonding and coordination interactions between the components. [fig 5-6]

The FTIR spectrum of pure quercetin displays characteristic peaks attributed to –OH stretching around 3400 cm^{-1}, C=O stretching at approximately 1650 cm^{-1}, and aromatic C=C stretching between 1600–1500 cm^{-1}, which correspond to the typical functional groups in flavonoids. In the nanocomposite formulations (NCCQ2, NCCQ3), these peaks show noticeable shifts and changes in intensity. Such spectral variations indicate molecular-level interactions between quercetin, carboxymethyl cellulose (CMC), and halloysite clay. Additionally, new peaks appearing in the 1030–1100 cm^{-1} range are indicative of Si–O stretching vibrations, confirming the presence of halloysite. These spectral changes collectively confirm the successful encapsulation of quercetin into the polymer–clay matrix, suggesting hydrogen bonding and physical entrapment as the likely mechanisms of incorporation. [fig 7-8]

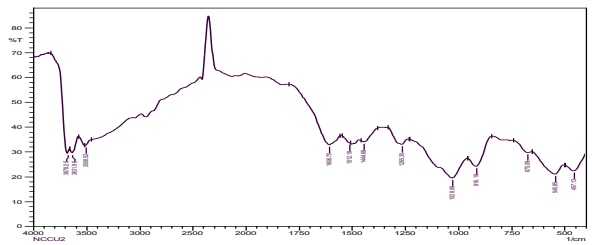

Figure 5: FTIR Spectra for pure curcumin

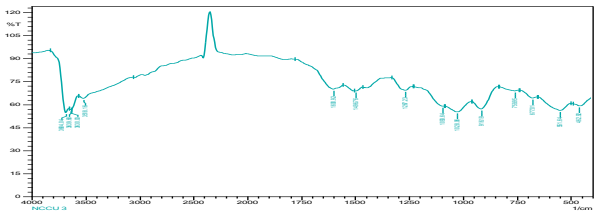

Figure 6: FTIR Spectra for curcumin nanocomposites

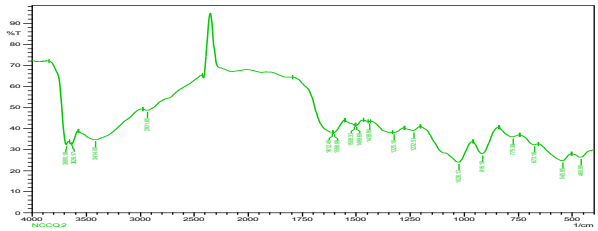

Figure 7: FTIR Spectra for pure quercetin

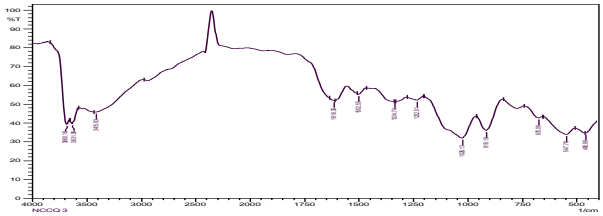

Figure 8: FTIR Spectra for quercetin nanocomposites

Scanning electron microscopy

The SEM images revealed a heterogeneous surface with embedded particulate structures, indicating the successful incorporation of drug and clay within the CMC matrix. The nanocomposites exhibited a relatively dense and compact morphology, with smoother and more continuous surfaces as clay loading increased. This suggests enhanced interaction between the polymer chains and clay, promoting better dispersion and network formation within the matrix. The coating observed over the particles indicates effective encapsulation of curcumin or quercetin. No visible crystalline drug particles were observed on the surface, supporting the inference that the drug was well distributed or molecularly dispersed within the matrix. Overall, the morphological features confirm successful nanocomposite formation and suggest a structure favorable for sustained and uniform drug release. [Fig-9-12]

Figure 9: Scanning electron microscopy of pure curcumin

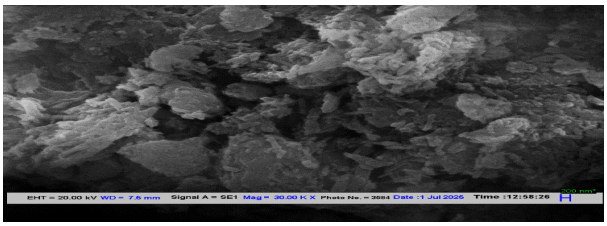

Figure 10: Scanning electron microscopy of curcumin nanocomposites

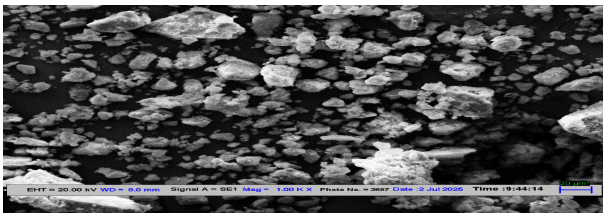

Figure 11: Scanning electron microscopy of pure quercetin

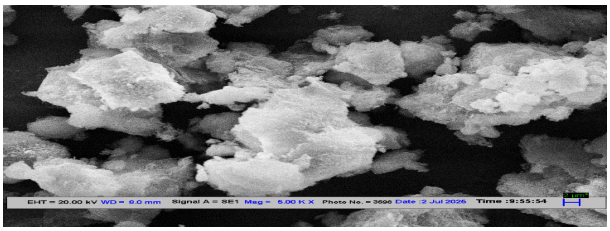

Figure 12: Scanning electron microscopy of quercetin nanocomposites

X-ray Diffraction (XRD)

X-ray diffraction (XRD) analysis was performed using a Cu Kα source (λ = 1.5418 Å) over a 2θ range of 5°–80° to investigate the crystalline characteristics of pure curcumin, quercetin, and their nanocomposite formulations. Diffractograms were recorded at a scanning rate of 2°/min. The characteristic sharp peaks of pure curcumin and quercetin observed at specific 2θ angles confirmed their crystalline nature. In contrast, the nanocomposite formulations displayed significant peak broadening and reduced intensity, indicating a partial loss of crystallinity due to molecular dispersion within the halloysite–CMC matrix. This reduction in crystallinity suggests successful encapsulation and potential improvement in solubility and bioavailability of the bioactive. [fig13-14]

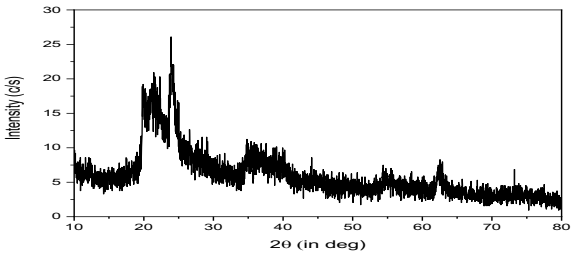

Figure 13: XRD Diffractograms for pure curcumin

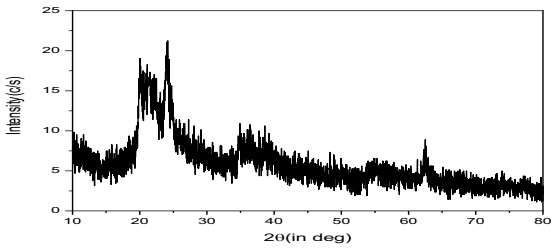

Figure 14: XRD Diffractograms for pure quercetin

Differential Scanning Calorimetry (DSC)

DSC thermograms of pure curcumin and quercetin exhibited sharp endothermic peaks at around 175°C (curcumin) and 320°C (quercetin), corresponding to their respective melting points, confirming their crystalline nature. In the nanocomposite formulations, these melting endotherms were either shifted, significantly broadened, or reduced in intensity. Specifically, the endothermic peak of curcumin was either masked or merged with broader transitions, while the sharp peak of quercetin was notably diminished. This suggests a reduction in crystallinity and possible molecular dispersion of the actives within the halloysite–CMC matrix. The halloysite–CMC carrier system displayed broad transitions around 149°C and 220°C, which may correspond to matrix relaxation or dehydration events, further supporting successful drug encapsulation and interaction. The absence or broadening of drug melting peaks in the nanocomposites indicates decreased crystallinity, potentially contributing to improved solubility and thermal stability of the formulation. [Fig 15-16]

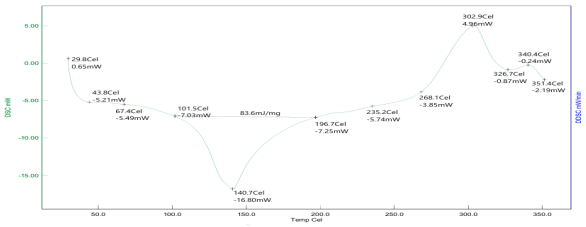

Figure 15: DSC thermograms of pure curcumin

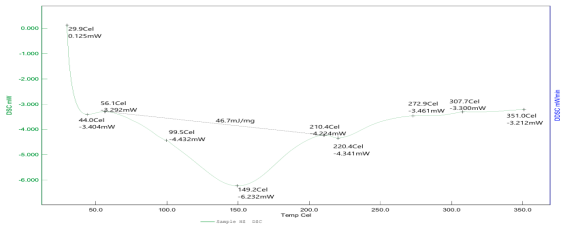

Figure 16: DSC thermograms of pure quercetin

In Vitro Drug Release study of nanocomposite formulation

The in vitro drug release profiles of curcumin and quercetin from the nanocomposite tablets are presented in Figure 17 and Figure 18, respectively. The release study demonstrated a gradual and controlled release pattern for both drugs over the experimental period. Curcumin exhibited a sustained release behavior, characterized by an initial moderate release followed by a steady increase in cumulative percentage release with time. This pattern indicates effective incorporation of the drug within the halloysite–CMC nanocomposite matrix, resulting in diffusion-controlled release. Similarly, quercetin showed a consistent and controlled release profile without abrupt burst release, suggesting uniform drug distribution within the nanocomposite system. The release kinetics indicate that the polymer–clay network effectively modulated drug diffusion into the dissolution medium. Overall, the release profiles confirm the ability of the developed nanocomposite formulation to provide sustained and controlled delivery of both curcumin and quercetin, thereby supporting its potential application in advanced drug delivery systems.

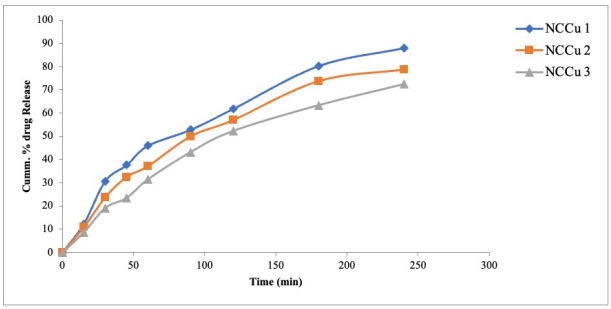

Figure 17: *In vitro* drug release for curcumin nanocomposites

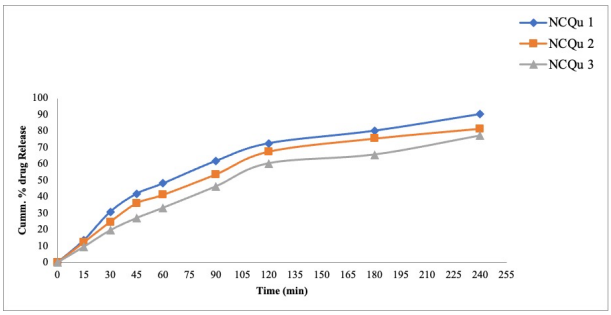

Figure 18: *In vitro* drug release for quercetin nanocomposites

Conclusion

The study demonstrates that halloysite–CMC nanocomposites offer an effective platform for the dual delivery of curcumin and quercetin. The engineered nanocomposites exhibited favorable drug–matrix interactions, reduced crystallinity, and controlled release profiles, addressing the inherent solubility and stability challenges of both bioactives. These findings support the potential of halloysite–based nanocomposites as a promising strategy for improving the biopharmaceutical performance of hydrophobic phytoconstituents in oral delivery applications.

Acknowledgments

The authors gratefully acknowledge the support provided by the RKU University, Rajkot, India, Central Research Facility, Indian Institute of Technology, Delhi, India

Financial Assistance

None

Conflict of Interest

The author declares no conflict of interest.

Author Contribution

The research, including study design, data collection, analysis, and manuscript drafting, was conducted by Amol Sonawane. Dr. Vaibhavi Savalia provided direction, oversight, and essential edits to the manuscript. The final draft of the paper was examined and approved by both authors.

References

1. Aggarwal, B.B., et al. (2007). Curcumin: The Indian solid gold. Adv Exp Med Biol, 595, 1–75.
2. Boots, A.W., et al. (2008). Health effects of quercetin: From antioxidant to nutraceutical. Eur J Pharmacol, 585(2-3), 325–337.
3. Gupta, S.C., et al. (2013). Multitargeting by curcumin as revealed by molecular interaction studies. Nat Prod Rep, 30(3), 394–404.

4. Hatcher, H., et al. (2008). Curcumin: From ancient medicine to current clinical trials. Cell Mol Life Sci, 65(11), 1631–1652.
5. Hewlings, S.J., & Kalman, D.S. (2017). Curcumin: A review of its effects on human health. *Foods*, 6(10), 92.
6. Li, Y., et al. (2016). Quercetin, inflammation and immunity. Nutrients, 8(3), 167.
7. Russo, M., et al. (2012). Phytochemicals in cancer prevention and therapy. Biomed Res Int, 2012, 243516.
8. Anand, P., et al. (2007). Bioavailability of curcumin: Problems and promises. Mol Pharm, 4(6), 807–818.
9. D'Andrea, G. (2015). Quercetin: A flavonol with multifaceted therapeutic applications? Fitoterapia, 106, 256–271.
10. Anand, P., et al. (2008). Curcumin and cancer: An "old-age" disease with an "age-old" solution. Cancer Lett., 267(1), 133–164.
11. Moon YJ, Wang L, DiCenzo R, Morris ME. Quercetin pharmacokinetics in humans. Biopharm Drug Dispos. 2008;29(4):205-17. doi:10.1002/bdd.605
12. Shanmugam, M.K., et al. (2015). The multifaceted role of curcumin in cancer prevention and treatment. Molecules, 20(2), 2728–2769.
13. Panahi, Y., et al. (2015). Curcumin and quercetin: A potential therapeutic strategy in cancer chemotherapy. Pharmacol Res., 102, 74–89.
14. Shamsi, F., et al. (2020). Advances in nanotechnology-based curcumin delivery systems: A review. J Drug Deliv Sci Technol, 57, 101668.
15. Nabavi, S.F., et al. (2015). Nanotechnology for delivery of natural compounds: Recent progress and future perspectives. Curr Pharm Des, 21(23), 3310–3322.
16. Lvov, Y.M., et al. (2016). Halloysite clay nanotubes for controlled release applications. Expert Opin Drug Deliv, 13(4), 489–503.
17. Cavallaro, G., et al. (2017). Halloysite nanotubes for drug delivery: Recent advances and future perspectives. J Control Release., 264, 302–316.
18. Lvov YM, Shchukin DG, Möhwald H, Price RR. Halloysite clay nanotubes for controlled release of protective agents. ACS Nano. 2008 May;2(5):814-20. doi: 10.1021/nn800259q. PMID: 19206476.
19. Lvov Y, Wang W, Zhang L, Fakhrullin R. Halloysite Clay Nanotubes for Loading and Sustained Release of Functional Compounds. Adv Mater. 2016 Feb 10;28(6):1227-50. doi: 10.1002/adma.201502341. Epub 2015 Oct 6. PMID: 26438998.
20. Yendluri R, Otto DP, De Villiers MM, Vinokurov V, Lvov YM. Application of halloysite clay nanotubes as a pharmaceutical excipient. Int J Pharm. 2017 Apr 15;521(1-2):267-273. doi: 10.1016/j.ijpharm.2017.02.055. Epub 2017 Feb 21. PMID: 28235623.
21. Rabea, E.I., et al. (2021). Carboxymethyl cellulose: Properties and applications in drug delivery. Int J Biol Macromol, 172, 585–597.
22. Savjani KT, Gajjar AK, Savjani JK. Drug solubility: importance and enhancement techniques. ISRN Pharm. 2012;2012:195727. doi:10.5402/2012/195727.
23. Dhanaraju MD, Reddy PR, Mallikarjun R. Solubility enhancement techniques of polyphenolic compounds for oral delivery – a review. Res J Pharm Tech. 2020;13(6):2891-2896. doi:10.5958/0974-360X.2020.00512.0.
24. Priyadarsini KI. The chemistry of curcumin: from extraction to therapeutic agent. Molecules. 2014;19(12):20091-20112. doi:10.3390/molecules191220091.
25. Kumar S, Pandey AK. Chemistry and biological activities of flavonoids: an overview. ScientificWorldJournal. 2013 Dec 29;2013:162750. doi: 10.1155/2013/162750. PMID: 24470791; PMCID: PMC3891543.
26. OECD Guidelines for the Testing of Chemicals. Partition Coefficient (n-octanol/water): Shake Flask Method. OECD Publishing; 2004.
27. Martin A, Sinko PJ. Martin's Physical Pharmacy and Pharmaceutical Sciences. 6th ed. Lippincott Williams & Wilkins; 2010.
28. Mishra B, Patel BB, Tiwari S. Colloidal carriers for solubility enhancement of poorly water-soluble drugs: review. Asian J Pharm Sci. 2014;9(6):244-253. doi:10.1016/j.ajps.2014.04.005.
29. Harborne JB. Phytochemical Methods: A Guide to Modern Techniques of Plant Analysis. Springer; 1998.
30. Siddiqui S, Verma A, Rather AA, Jabeen F, Meghvansi MK. Preliminary phytochemicals screening of crude extracts of Moringa oleifera leaves. J Pharmacogn Phytochem. 2013;1(6):1-5.
31. Trease GE, Evans WC. Pharmacognosy. 16th ed. Saunders; 2009.